WILEY-VCH

Supported Ruthenium Single-Atom and Clustered Catalysts Outperform Benchmark Pt for Alkaline Hydrogen Evolution

Yanping Zhu, Ke Fan, Chia-Shuo Hsu, Gao Chen, Changsheng Chen, Tiancheng Liu, Zezhou Lin, Sixuan She, Liuqing Li, Hanmo Zhou, Ye Zhu, Hao Ming Chen, Haitao Huang**

Dr. Y. Zhu, Dr. K. Fan, Dr. G. Chen, C. Chen, T. Liu, Z. Lin, Dr. S. She, L. Li, H. Zhou, Prof. Y. Zhu, Prof. H. Huang
Department of Applied Physics and Research Institute for Smart Energy, The Hong Kong Polytechnic University, Hong Kong, China
E-mail: aphhuang@polyu.edu.hk

Dr. C.-S. Hsu, Prof. H. M. Chen
Department of Chemistry, National Taiwan University, Taipei 106, Taiwan
E-mail: haomingchen@ntu.edu.tw

Prof. H. M. Chen
National Synchrotron Radiation Research Center, Hsinchu 30076, Taiwan

Prof. H. M. Chen
Graduate Institute of Nanomedicine and Medical Engineering, College of Biomedical Engineering, Taipei Medical University, Taipei 11031, Taiwan

Keywords: single atom, nanocluster catalysts, density functional theory, operando characterization, alkaline hydrogen evolution

Guaranteeing satisfactory catalytic behavior while ensuring high metal utilization has become the problem that needs to be addressed when designing noble metal based catalysts for electrochemical reactions. Here, the well-dispersed ruthenium (Ru) based clusters with adjacent Ru single atoms (SAs) on layered sodium cobalt oxide (Ru/NC) is demonstrated to be a superb electrocatalyst for alkaline HER. The Ru/NC catalyst manifests an activity increase by a factor of two relative to the commercial Pt/C. *Operando* characterizations in conjunction with density

functional theory (DFT) simulations uncover the origin of the superior activity and establish a structure-performance relationship, that is, under HER condition, the real active species are Ru SAs and metallic Ru clusters supported on the NC substrate. The excellent alkaline HER activity of the Ru/NC catalyst can be understood by a spatially decoupled water dissociation and hydrogen desorption mechanism, where the NC substrate accelerates the water dissociation rate, and the generated H intermediates would then migrate to the Ru SAs or clusters and recombine to have H_2 evolution. More importantly, comparing the two forms of Ru sites, it is the Ru cluster that dominates the HER activity.

1. Introduction

Electrochemical water splitting has been widely acknowledged as the cleanest technology for hydrogen generation.[1-5] Typically, the state-of-art catalysts are based on the noble platinum and ruthenium/iridium for cathodic hydrogen evolution reaction (HER) and anodic oxygen evolution reaction (OER), respectively. Recent years have witnessed the tremendous efforts involved in developing earth-abundant and low-cost materials to replace precious-metal based electrocatalysts. For instance, the Ni-Fe based catalysts have demonstrated OER performance comparable with ruthenium oxide,[6-8] while for the HER side, most of nonprecious-metal-based catalysts still show far inferior performance to the noble metal catalyst (such as Pt, ruthenium (Ru), rhodium (Rh), and gold (Au)).[9-11] Considering the scarcity and high cost of noble metals, reducing the amount used and make the best of these noble resources remain the most challenging when designing alternative electrocatalysts for alkaline HER.

To enable more atoms to participate in the designed catalytic reaction, one obvious approach is to downsize a bulk catalyst to nanoparticle, nanocluster or even single atom as the ultimate limit. With the decrease of catalyst size, the number of surface atoms exposed is profoundly increased, together with an alteration of the surface atomic structure, electronic structure and surface defects, which have aroused increasing research interests in the field of heterogeneous catalysis.[12-14] Theoretically, noble metal single atom catalyst (NMSAC) with the maximum atom utilization efficiency (100%) should meet the urgent need for the best use of noble resource. However, when catalyzing the HER, the activities of most of the reported NMSAC remain lower than the benchmark and even the conventional nanoparticle catalysts. A major reason is that the metal content in the current NMSAC is very low (< 1 wt%), where the individual atoms may easily migrate and agglomerate into larger clusters due to the high specific surface energy of single atom in NMSACs.[15-17] Moreover, when preparing NMSACs, additional physical/chemical treatment such as acid leaching may be involved to remove

impurities and unstable nanoparticles, which would induce a possible waste of precious metals and a decreased yield.[16] Therefore, how to guarantee satisfactory catalytic behavior while ensuring the high metal utilization becomes one of the challenging problems that needs to be addressed.

Generally, HER rate in alkaline media is 2-3 orders of magnitude lower than that in acidic condition. The sluggish alkaline HER can be attributed to the insufficient proton supply from slow water dissociation.[18-20] Although the Pt-group metals have optimal hydrogen adsorption free energy, they are generally inefficient in the prior step of water dissociation. Conversely, metal oxide/hydroxide are efficient for cleaving HO-H bond, but are poor in the other essential processes of hydrogen adsorption and H_2 desorption. Hence, an ideal alkaline HER catalyst should combine the catalytic proficiencies of metal oxide/hydroxide and Pt-group metals to create bifunctional effects.[21-24] A well-known example is the Pt/$Ni(OH)_2$ hybrid which yields 8 times higher HER activity than pristine Pt, in which the overall multistep HER in alkaline solution was facilitated by the strategic combination of water-dissociating $Ni(OH)_2$ and H-combing Pt.[25] This success represents a breakthrough in improving the sluggish kinetics for electrochemical reduction of water to molecular hydrogen in alkaline environments.

Noble metal ruthenium (Ru) shares similar property with Pt and possesses the merits of relatively low cost (~4% cost of Pt), thereby becoming an idea alternative to Pt for HER.[26-28] In this work, through a facile cation exchange reaction under room temperature, we constructed a supported ruthenium catalyst with dual local structures in which amorphous Ru hydroxide clusters with neighboring Ru SAs were well dispersed and supported on the layered sodium cobalt oxide ($NaCoO_2$, NC). The hybrid catalyst (denote as Ru/NC) achieved superior performance towards alkaline HER. More importantly, its mass activity (4.67 A mg^{-1} at -0.2 V vs RHE) was nearly twice that of the commercial 20% Pt/C, demonstrating its great potential for practical application. *Operando* X-ray absorption spectroscopy (XAS) was carried out to capture the dynamic structural evolution under HER condition, from which we could draw a clear conclusion that the obtained Ru/NC catalyst may act as the "pre-catalyst" rather than the real active species, and the reactive species were Ru SAs and metallic Ru clusters in HER condition. In addition, density functional theory (DFT) calculations elucidated how the individual component of Ru/NC cooperated to enhance the HER activity in alkaline environment. Briefly, the $NaCoO_2$ substrate provided active sites for dissociation of water, and the generated H intermediates (H*) recombined to generate H_2 on the Ru SAs or clusters. Comparing the two kinds of Ru sites, Ru cluster dominated the HER activity due to the more fluent migration of H* and its more favorable adsorption-desorption energetics towards H

intermediates. This study inspires us to pursue a balance between atomic utilization and performance when developing noble metal catalysts for alkaline HER.

2. Results and discussion

The Ru based species dispersed on NC substrate was facilely synthesized by a cation exchange reaction under room temperature. Due to the weak acidity of $RuCl_3$ aqueous solution, H^+ would attack the alkaline Na^+ ions between CoO_2 slabs in $NaCoO_2$. The smaller radius of Ru^{3+} ion (0.82 Å) than that of Na^+ (1.02 Å) allows easy access for Ru ions into the interlayer space of $NaCoO_2$. As a result, the Ru species would be deposited on the surface of CoO_2 slabs with the layered $NaCoO_2$ exfoliated simultaneously. Corresponding XRD patterns of the NC and Ru/NC samples were displayed in **Figure 1a**. After Ru treatment, the diffraction peaks of the Ru/NC catalyst were still indexed well with the hexagonal $NaCoO_2$ phase (JCPDS no. 00-030-1182). Compared with the pristine NC, its peak intensity was reduced and its peak location shifted to lower diffraction angles, implying an enlarged interlayer spacing in the Ru/NC structure. No additional peaks assigned to Ru-related metals or oxides were observed. The broad peak at about 18° should be assigned to the amorphous Ru hydroxide deposited on the NC surface. Field-emission scanning electron microscopy (FESEM) and high angle annular dark-field scanning transmission electron microscopy (HAADF-STEM) were employed to reveal the general morphology and textural details of the as-prepared catalysts. As expected, the NC sample displayed agglomeration of large particles resulted from the high-temperature calcination (Figure S1). The Ru treatment significantly changed its morphology. As observed in Figure S2, the sheet-like structure in the cross-sectional view of the Ru/NC sample indicated the successful exfoliation of the bulk NC. Numerous clusters with an average size of ~ 1 nm were found monodispersed on the substrate (Figure 1b). High-resolution transmission electron microscopy (HRTEM) image of the substrate in Figure 1c showed continuous lattice spacing of 0.528 nm corresponding to the (002) plane of $NaCoO_2$. The larger lattice distance of NC substrate in Ru/NC than that of the pristine NC (0.514 nm, Figure S3) suggested the expansion of layer spacing after the Ru treatment, which agreed well with the XRD results. The reduced crystallinity of NC substrate is attributed to the partial etching in acidic Ru solution, which is consistent with the reduced XRD peak intensity of the Ru/NC sample. Moreover, the HAADF-STEM image of the Ru/NC (Figure 1d) showed that the disordered Ru hydroxide clusters (highlighted by blue ellipses) existed with neighboring Ru single atoms (highlighted by red circles), and the elemental mapping displayed in Figure 1e demonstrated uniform distribution of Ru across the region selected. The Ru content was ~11.2 wt% as determined by the

inductively coupled plasma mass spectrometry (ICP-MS) measurement (Table S1). Then X-ray absorption spectroscopy (XAS) was conducted with the aim of unveiling the coordination environment of Ru and Co in the as-prepared Ru/NC sample. As observed from the corresponding Ru K-edge Fourier-transformed extended X-ray absorption fine structure (FT-EXAFS) spectrum of the Ru/NC (Figure 1f), the dominate peak at 1-2 Å was assigned to the Ru-O contribution. The broad coordinated shell at approximately 3 Å consisted of Ru-O-Co and Ru-O-Ru contributions attributed to Ru single atom and Ru hydroxide clusters, respectively. The presence of metallic Ru and crystalline RuO_2 can be excluded. Figure 1g displayed the FT-EXAFS spectra of Co K-edge for the NC and Ru/NC samples. The scattering peaks at 1-2 and 2-3 Å were attributed to Co-O and Co-Co contributions, respectively, in the CoO_2 slab of $NaCoO_2$. Quantitative analysis was summarized in Figure S4 and Table S2. It was worth to be noted that the multiple scattering Co-M peaks of the Ru/NC all shifted to the larger distance than those of pristine NC, which confirmed again the enlarged layer spacing of NC after the Ru treatment. The above analysis identified the exfoliated CoO_2 slabs as well as the coexistence of Ru based single atom and cluster in the Ru/NC (Figure 1h). In addition, the nitrogen adsorption-desorption curves (Figure S5a and S5b) of the bulk NC demonstrated a type-III isotherm without hysteresis loops, indicating its non-porous nature. On the contrary, the type-IV isotherm with H_3 hysteresis loops from the Ru/NC materials (Figure S5c and S5d) suggested the presence of rich mesopores. Significantly, the Ru/NC sample possessed a much higher specific area of 31.12 $m^2\ g^{-1}$ and a larger total pore volume of 0.11 $cm^3\ g^{-1}$ than those of the pristine NC (3.45 $m^2\ g^{-1}$ and 0.008 $cm^3\ g^{-1}$). It was anticipated that such highly porous microstructure would allow easy penetration of electrolyte and expose a large number of active sites during the electrocatalysis.[29,30]

The electrocatalytic performance of the as-prepared Ru/NC composite toward HER was assessed in a 1 M KOH electrolyte involving a three-electrode system. Similar evaluations were carried out on pristine NC, metallic Ru on conductive carbon support (Ru/C) and commercial 20 wt% Pt/C for direct comparison. **Figure 2a** recorded the typical polarization curves of the four catalysts. As expected, the Pt/C electrode demonstrated highly active HER performance with the lowest onset overpotential (U_{onset}) of near zero and an overpotential of only 24 mV to reach 10 mA cm^{-2} (η_{10}), which agreed well with the previous reports.[31,32] The pristine NC catalyst showed rather poor HER performance as indicated by a large U_{onset} value of 200 mV and a large η_{10} value of 313 mV. In stark contrast, after Ru treatment, the Ru/NC electrode had a dramatically decreased onset overpotential of nearly zero volt and a reduced overpotential of 25 mV to achieve 10 mA cm^{-2}. Such performance is almost the same as that of the benchmark

Pt/C and significantly outperforms most of the alkaline HER catalysts (Table S3). Meanwhile, to determine the optimal Ru content for the Ru/NC composite electrode, three other catalysts synthesized under different Ru concentrations were prepared and denoted as Ru_4/NC, Ru_8/NC and Ru_{16}/NC. With the increase of exchanged Ru amount, diffraction peaks from the XRD patterns decreased in intensity (Figure S6), which was probably attributed to the increasing dissolution of NC structure in the H^+ environment. After electrochemical assessment, the Ru_{12}/NC electrode (also Ru/NC as mentioned before) showed the best performance when catalyzing the HER (Figure S7), suggesting the existence of an optimum content of Ru species for the best HER performance. Moreover, metallic Ru supported on conductive carbon support with the same Ru content to the Ru/NC composite was prepared. The corresponding XRD pattern (Figure S8) confirmed its metallic Ru phase. As observed from the TEM image of the Ru/C material (Figure S9), numerous nanosized particles were uniformly distributed on the conductive carbon support. However, the Ru/C catalyst exhibited much inferior HER activity to the Ru/NC. It needed an overpotential of 86 mV to drive 10 mA cm^{-2}, 61 mV more than the Ru/NC, which indicated a synergistic effect between the Ru species and the NC substrate in the HER condition. Ru SAs distributed on the NC support was also prepared under low Ru concentration (Ru SA/NC, Figure S10a), and the catalyst demonstrates far inferior activity than the Ru/NC (Figure S10b). Mass activity is an important issue that is closely related to the cost of catalyst. Figure 2b plotted the mass activity (normalized to mass of Ru or Pt) of the samples at an overpotential of 0.2 V. The Ru/NC electrode delivered a mass activity of 4.67 A mg^{-1}, which is 5.2 and 1.9 times that of the Ru/C and Pt/C catalysts, respectively, indicating its greater advantage for practical applications. Besides, the price activity (normalized to price of Ru or Pt) for the Ru/NC electrode is 38 times greater than that of the commercial Pt/C, demonstrating that the Ru/NC catalyst is cost-efficient. Figure 2c displayed Tafel plots of the catalysts. A Tafel slope of 29 mV dec^{-1} was obtained for the Ru/NC electrode, which was close to the benchmark Pt/C (26 mV dec^{-1}) but markedly smaller than those of Ru/C (88 mV dec^{-1}) and bulk NC (159 mV dec^{-1}). Notably, Tafel analysis should be made in strong polarization regime where the reverse reaction proceeds at sufficiently slow rate and thus can be neglected. If the electrode kinetics are fairly facile, the system will approach the mass-transfer-limited current by the time such an extreme overpotential (overpotential > 100 mV/n) is established. Tafel relationships cannot be observed for such cases, because they require the absence of mass-transfer effects on the current.[33,34] As shown in the Pt/C and Ru/NC cases, the curves exhibits high slope and inferior linearity at large overpotentials. Theoretically, there are no obvious Tafel region for these catalysts. The low overpotential windows for kinetic analysis in this study as well as the

previous reports should be pseudo-Tafel regions.[35] According to the three principle steps in alkaline hydrogen evolution, hydrogen generation on the Ru/NC electrode proceeded *via* the Volmer-Tafel mechanism, while that on the other two electrodes followed the inefficient Volmer-Heyrovsky pathway.[3-5] We further compared the electrochemically active surface area (ECSA) of each catalyst, which was estimated from the double-layer capacitance (C_{dl}, Figure S11).[36] The Ru/NC catalyst had the largest C_{dl} value that was nearly 13 and 1.6 times that of the original NC and commercial Pt/C, respectively (Figure 2d), demonstrating the significantly enlarged ECSA after Ru treatment. Figure S12 exhibits the polarization curves of the three catalysts after normalizing to their corresponding ECSA. It was found that the HER activity of the Ru/NC catalyst was much better than the pristine NC and close to the benchmark Pt/C, implying the great improvement of its intrinsic activity. Finally, chronopotentiometric curves for the Ru/NC electrode were recorded at a fixed current density of 10 mA cm^{-2} to assess its long-term stability. Apparently, the applied potential remained identical for nearly 40 hours at least, revealing the robust stability of the catalyst.

It has been acknowledged that most catalysts would undergo structure reconstruction during the electro-derived oxidation or reduction process.[37-39] In order to investigate the structure evolution of catalysts during the catalytic process, *operando* X-ray absorption spectroscopy (XAS) was conducted on the Ru/NC electrode under HER conditions. **Figure 3a** showed the *in situ* Ru K-edge X-ray absorption near edge spectroscopy (XANES) spectra collected from the Ru/NC in conditions of as-prepared (A.P.), immersed into the KOH electrolyte (KOH), and cathodically increased potentials. The average oxidation state of Ru in the as-prepared Ru/NC catalyst is lower than +4 as its absorption edge shifted to lower energy than that of the reference RuO_2. The chemical state of Ru remained the same upon contacting with the alkaline electrolyte. After progressively increasing the cathodic potential, the absorption edge position had a pronounced shift toward that of Ru foil, suggesting the reduced oxidation state of Ru during the HER. As plotted in Figure 3b, the Ru of the as-prepared Ru/NC is characteristic of an average valence of +3.7, whereas the oxidation state decreased to approximately +2.0 under HER potentials. Evolution of the coordinated environment of absorbing Ru was further extracted by *operando* EXAFS spectra (Figure 3c). Upon applying HER potentials, the decreased peak intensity of Ru-O contribution and the enlarged Ru-O bond length corresponded to the reduced Ru valence state. More importantly, the peak that corresponded to Ru-O-Ru contributions in the Ru hydroxide clusters gradually faded, and simultaneously, a new scattering path that attributed to the Ru-Ru path in metallic Ru emerged, indicating the generation of Ru clusters. The state of single atom for Ru was well maintained in HER condition, which was evidenced

by the average oxidation state of Ru (+2). The corresponding quantitative analysis summarized in Figure S13 and Table S3 agreed well with these findings. When increasing the applied potential back to open circle voltage (OCV), the Ru cluster still maintained (Figure S14a), indicating the irreversibility of the process. According to the corresponding curve fitting results in Figure S14b&c and Table S3, compared with that of the "-0.28 V" condition, the slightly increased CN value of Ru-O and the shortened Ru-O bond length in the "OCV-back" spectrum might be ascribed to the reoxidation by electrolyte. Meanwhile, the Ru-Ru contribution for Ru cluster and the Ru-Co for Ru SAC were almost unchanged. Also, *in situ* Co K-edge XANES and EXAFS spectra were analyzed to probe the structure transformation of the $NaCoO_2$ substrate (Figure S15). Notably, neither the oxidation state nor the coordination environment of Co showed obvious change during the HER, demonstrating the robust structure stability of $NaCoO_2$ support in the Ru/NC composite catalyst. The above findings clearly revealed that during the HER process, the obtained Ru/NC catalyst may act as the "pre-catalyst" rather than the real active species. The Ru hydroxide cluster was easily reduced to metallic Ru cluster, and the reactive species were Ru SAs and Ru clusters in HER condition (Figure 3d).

To gain comprehensive insights into the enhanced HER performance by the Ru/NC catalyst, CV curves for the NC, Ru/NC and Ru/C electrodes were recorded in 0.1 M KOH (Figure S16). The onset of OH adsorption (OH_{ads}) started at more negative potentials on the Ru/NC electrode, implying a better interaction with the incoming H_2O compared to the Ru/C.[24,25,40] This demonstrated a more efficient dissociative adsorption of water molecules with the help of NC substrate. It was found that the Ru/NC curve had no distinct peak for under-potential deposited hydrogen (H_{upd}) as that in the Ru/C, which was probably ascribed to the atomic-level distribution of Ru in the Ru/NC catalyst.[40] Given the real active sites and the superior activity of Ru/NC catalyst, we further performed DFT calculations to establish a structure-performance relationship of electrocatalysts and uncover the origin of the outstanding HER activity. In most studies, the computational models employed are the ideal atomic configuration based on the "initial state of catalyst" without considering the dynamic evolution of catalyst structure under applied bias, which may provide doubtful evaluations. In this regard, Ru SAs and Ru clusters (rather than Ru SAs and Ru hydroxide clusters) supported on the NC support was constructed as the model in the following study. During the model construction for Ru SA, five possible high-symmetry adsorption sites on the NC substrate were taken into consideration as shown in Figure S17. After quantitatively evaluating the adsorption energies (E_{ad}) of each condition, S2 was determined as the most favorable adsorption site for Ru single atom due to its lowest E_{ad} value (Figure S18). For the Ru cluster, the coordination number (CN) of Ru-Ru under HER

condition was close to 3 from the curve fitting results, which was consistent with the octahedral geometry of Ru_6 nanoclusters.[41] According the previous report[42] and simulation optimization, we constructed a Ru_6 cluster on the NC substrate. **Figure 4a** and 4b displayed the top and side view of the Ru SAs and Ru cluster models on NC substrate, respectively. To elucidate how the individual component of Ru/NC cooperate to enhance the HER activity, we applied DFT calculations on Ru SA, Ru cluster and NC sites for the key steps in alkaline HER, including dissociating H_2O molecule into hydroxyl group (OH^-) and H apart, relaying the reactive hydrogen intermediates (H_{ads}) to adjacent sites, and recombining H_{ads} to produce H_2.[43,44] As shown in Figure 4c, the energy barrier for breaking the OH-H bond in water (ΔG_{H_2O}) was 1.41 eV on the NC substrate, which was significantly lower than those on the Ru SA (1.80 eV) and Ru cluster (2.75 eV) surface. This indicated that the NC surface could promote the sluggish Volmer step substantially and increase the rate of H_{ads} formation by orders of magnitude, which is consistent with the above Tafel slope analysis. After that, channeling H intermediates from NC support to the nearby Ru sites is also of great significance. Climbing image nudged elastic band (CI-NEB) method was used to calculate the energy barrier of H atom diffusion from NC substrate to the two kinds of Ru sites. As displayed in Figure 4d, the energy barrier is much lower in the Ru cluster case (0.76 eV), implying a much more feasible H migration. In the kinetic view, the rapid migration of H intermediates would guarantee an efficient H_2 generation.

Finally, hydrogen adsorption free energy on different sites were calculated. On the NC substrate surface, three high-symmetry possible sites (S1, S2, S3) for hydrogen atom adsorption have been discussed (Figure S19), from which it was found that the hydrogen atom preferred to adsorb on top of O atom (S2) while it could hardly remain stable on the other two sites during the geometric optimization. Similarly, the optimal adsorption sites for hydrogen adsorption at the Ru SA and Ru cluster surface were confirmed (Figure S20). Figure S1 displayed the Gibbs free energy for HER on the three sites. From a thermodynamic perspective, the Gibbs free energy change of hydrogen adsorption (ΔG_{H*}) should be close to zero as possible for an ideal HER catalyst.[45,46] As the hydrogen adsorption free energy on the NC substrate ($\Delta G_{H*} = -0.85$ eV) was much stronger than the optimal value ($\Delta G_{H*} = 0$ eV), the desorption of H_{ads} and H_2 production would be hindered. In contrast, it was found that the hydrogen adsorption free energies on the Ru SA and Ru cluster were much smaller and closer to the optimal value, which confirmed that the Ru SA and Ru cluster were responsible for the adsorption/combination of reactive H_{ads} to generate H_2. As revealed from the aforementioned Tafel analysis, the Ru/NC catalyst enabled the generation of hydrogen via a kinetically fast Volmer-Tafel process, where the relayed H_{ads} from NC would directly combine and desorb on the Ru sites. Gibbs free energy

diagrams following the Volmer steps on Ru SA and Ru cluster were calculated (Figure 4e). It was found that both ΔG_{H*} values for adsorbing the first H (-0.06 eV) and the second H (-0.07 eV) on the Ru cluster surface are very close to zero. In contrast, the second H adsorption is too strong on the Ru SA site with the calculated ΔG_{H*} value up to -0.70 eV, which greatly increased the difficulty of the Volmer reaction. Based on the above illustrations, it could be inferred that the synergy between NC substrate and Ru species rendered the Ru/NC composite an exceptional catalyst for alkaline HER. Specifically, the NC substrate accelerated the rate of water dissociation, and the generated H intermediates recombined to generate H_2 on the Ru SA or clusters. Considering the more fluent migration of H intermediates to Ru cluster, and the more favorable adsorption-desorption energetics toward H intermediates on the Ru cluster surface, it can be concluded that comparing the two kinds of Ru sites, Ru clusters dominate the HER activity (Figure 4f). These findings also explain the much inferior activity of the Ru SA/NC electrode.

3 Conclusion

In summary, on the basis of the above findings, the ruthenium catalyst with two existence forms supported on NC substrate has been demonstrated outstanding HER activity as well as robust stability in alkaline electrolyte. Individual role of each component of the Ru/NC hybrid catalyst when catalyzing HER was thoroughly discussed to establish a structure-performance relationship. This study highlights the importance of combining metal oxide support and Pt-group metal catalyst to create spatially decoupled water dissociation and hydrogen desorption towards efficient alkaline HER. Moreover, the more favorable activity of Ru cluster than Ru SA would inspire new direction in designing noble metal based catalysts with excellent performance for alkaline HER and beyond.

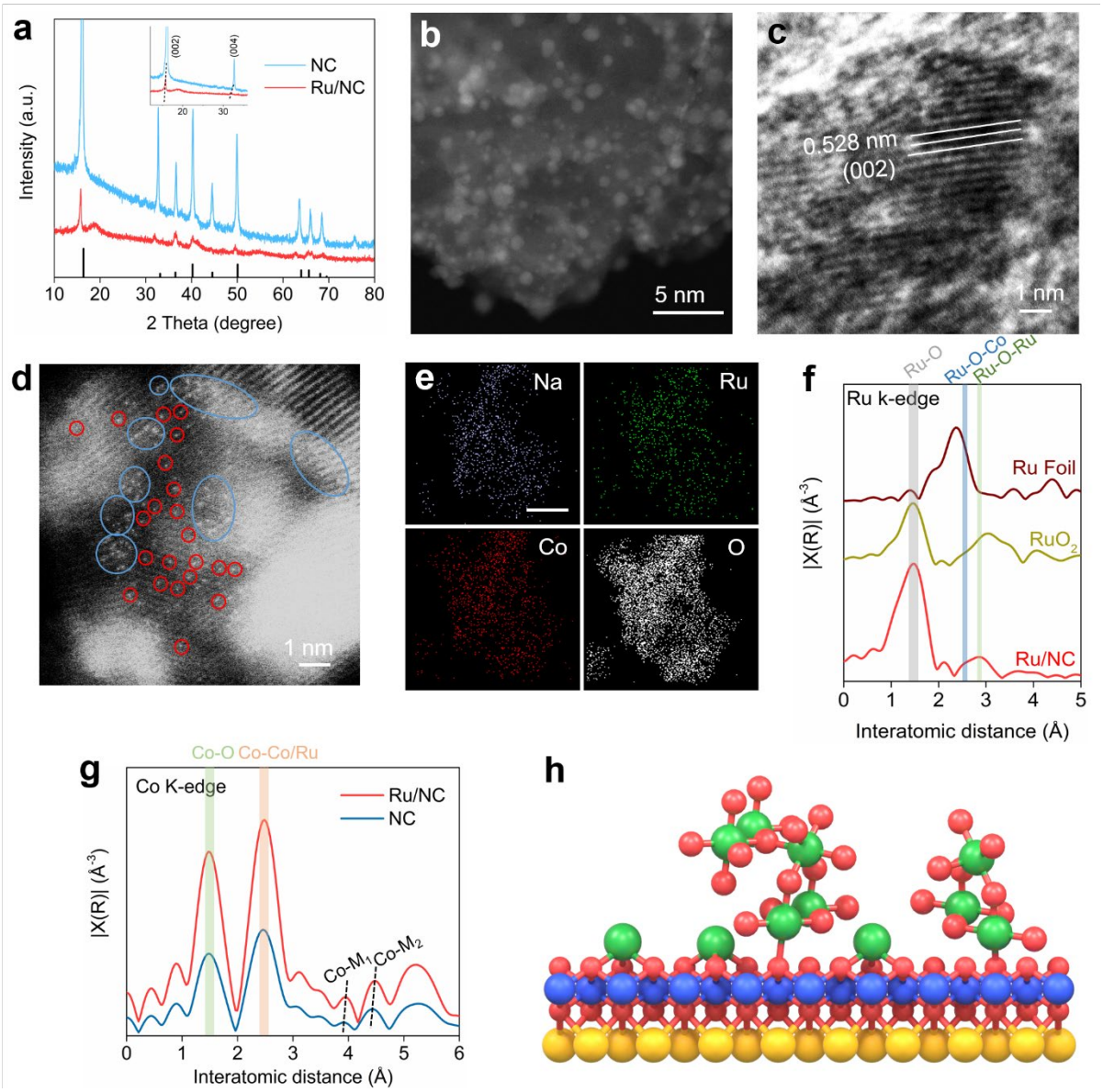

Figure 1. (a) XRD patterns of the NC and Ru/NC samples. The inset shows the magnified XRD pattern in the 2-theta range of 18-32°. (b) STEM and (c) HRTEM images of Ru/NC. (d) HAADF-STEM image and (e) element mapping of Ru/NC. The scale bar is 100 nm. (f) EXAFS spectra of Ru K-edge for the Ru/NC and references including RuO_2 and Ru foil. (g) EXAFS spectra of Co K-edge for the NC and Ru/NC. (h) Atomic configuration of the Ru/NC. The red, blue, yellow, and green balls represent O, Co, Na and Ru atoms, respectively.

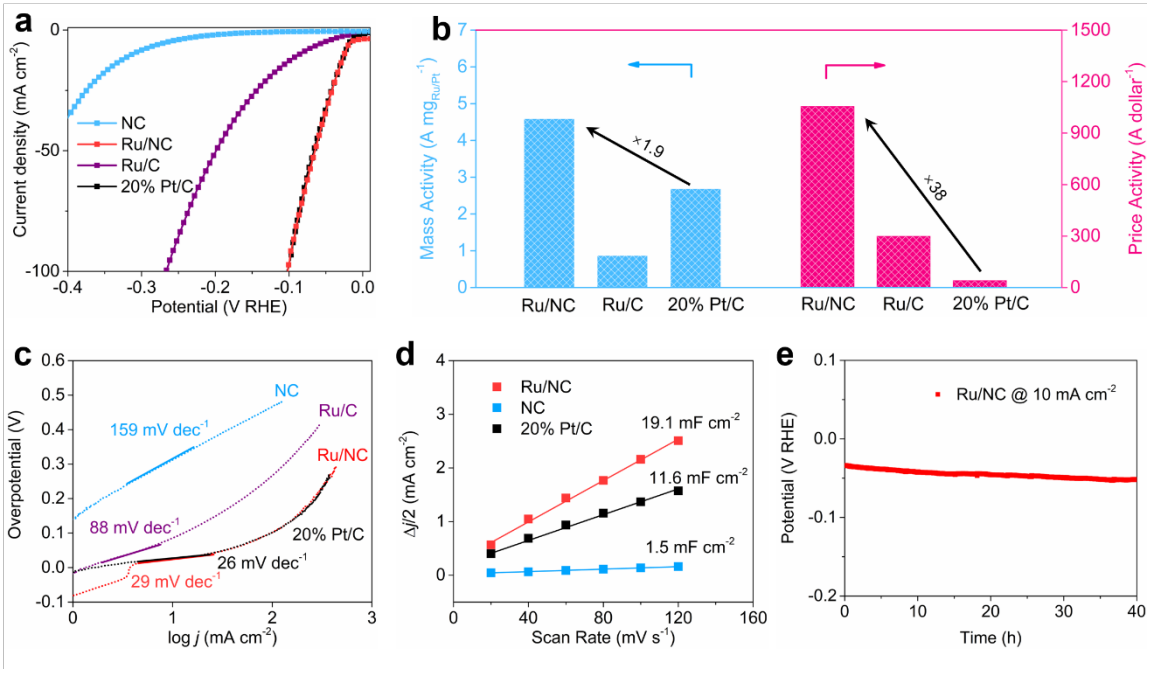

Figure 2. (a) HER LSV polarization curves, (b) calculated mass activity, price activity and (c) the corresponding Tafel plots of the NC, Ru/NC, Ru/C and commercial 20% Pt/C in 1 M KOH electrolyte. (d) Corresponding linear fitting of the capacitive currents versus CV scan rates for the NC and Ru/NC catalysts. (e) Chronopotentiometric curves of the Ru/NC at 10 mA cm^{-2}.

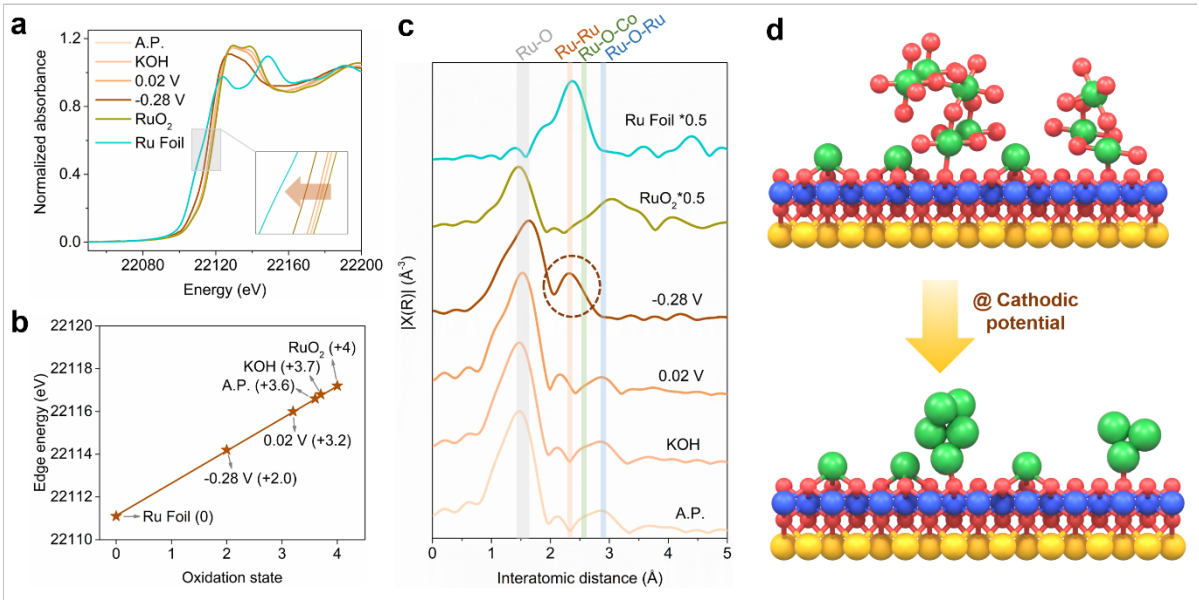

Figure 3. (a) *In-situ* Ru K-edge XANES spectra, (b) the oxidation state of Ru and (c) the corresponding EXAFS R-space spectra for the Ru/NC at various potentials for HER and references. (d) Schematic model of the structural transformation in Ru/NC toward HER.

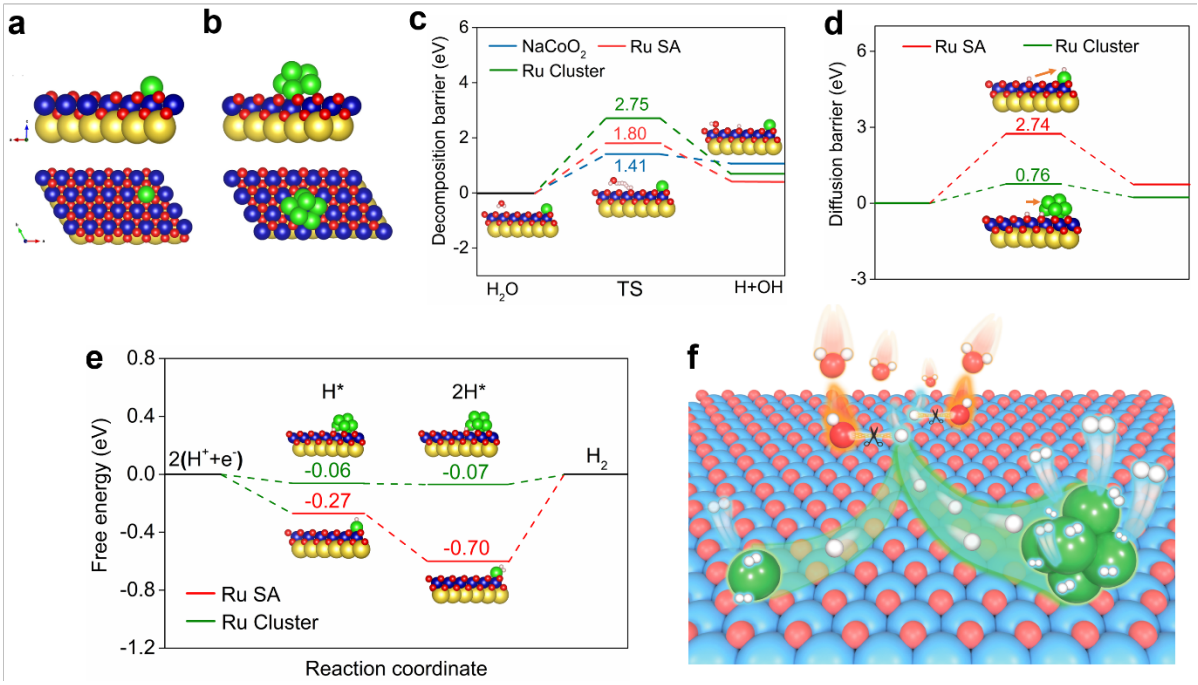

Figure 4. Top and side views of (a) Ru SA and (b) Ru cluster structures on NC support. (c) Kinetic energy barrier for water dissociation on NC, Ru SA and Ru cluster surface. Insets are the model structure for the initial state, transition state (TS) and final state. The red, pink, blue, yellow, and green ball represent O, H, Co, Na and Ru atoms, respectively. (d) Energy barriers for hydrogen migration from NC surface to the adjacent Ru SA and Ru cluster sites. (e) Gibbs free energy diagrams following the Volmer steps on Ru SA and Ru cluster. (f) Schematic diagram illustrating the role of each component in the Ru/NC when catalyzing the alkaline HER.

Supporting Information

Supporting Information is available from the Wiley Online Library or from the author.

Acknowledgements

Y. Zhu and K. Fan contribute equally to this work. This work was supported by the Research Grants Council of the Hong Kong Special Administrative Region, China (PDFS2223-5S03 and PDFS2122-5S02) and the Hong Kong Polytechnic University (1-ZE2F, 1-YY4A, Q-CDBG, 1-YWB6, and G-YWA1).

Conflict of Interest

The authors declare no conflict of interest.

Data Availability Statement

The data that support the findings of this study are available from the corresponding author upon resonable request.

Received: ((will be filled in by the editorial staff))
Revised: ((will be filled in by the editorial staff))
Published online: ((will be filled in by the editorial staff))

References

[1] T. F. Jaramillo, K. P. Jørgensen, J. Bonde, J. H. Nielsen, S. Horch, I. Chorkendorff, *Science* **2007**, *317*, 100-102.

[2] S. Chu, A. Majumdar, *Nature* **2012**, *488*, 294-303.

[3] Z.-Y. Yu, Y. Duan, X.-Y. Feng, X. Yu, M.-R. Gao, S.-H. Yu, *Adv. Mater.* **2021**, *33*, 2007100.

[4] J. Wei, M. Zhou, A. Long, Y. Xue, H. Liao, C. Wei, Z. J. Xu, *Nano-Micro Lett.* **2018**, *10*, 75.

[5] Y. Zheng, Y. Jiao, A. Vasileff, S.-Z. Qiao, *Angew. Chem. Int. Ed.* **2017**, *57*, 7568-7579.

[6] Q. Han, Y. Luo, J. Li, X. Du, S. Sun, Y. Wang, G. Liu, Z. Chen, *Appl. Catal. B: Environ.* **2022**, *304*, 120937.

[7] H. Lei, L. Ma, Q. Wan, S. Tan, B. Yang, Z. Wang, W. Mai, H. J. Fan, *Adv. Energy Mater.* **2022**, *12*, 2202522.

[8] N. Hashemi, S. Nandy, K. H. Chae, M. M. Najafpour, *ACS Appl. Energy Mater.* **2022**, *5*,

11098-11112.

[9] C. Li, J.-B. Baek, *ACS Omega* **2020**, *5*, 31-40.

[10] O. Jung, M. N. Jackson, R. P. Bisbey, N. E. Kogan, Y. Surendranath, *Joule* **2022**, *6*, 476-493.

[11] Y. Liu, Q. Wang, J. Zhang, J. Ding, Y. Cheng, T. Wang, J. Li, F. Hu, H. B. Yang, B. Liu, *Adv. Energy Mater.* **2022**, *12*, 2200928.

[12] Y. Yang, Y. Yang, Z. Pei, K. H. Wu, C. Tan, H. Wang, L. Wei, A. Mahmood, C. Yan, J. Dong, S. Zhao, Y. Chen, *Matter* **2020**, *3*, 1442-1476.

[13] C. Zhu, S. Fu, Q. Shi, D. Du, Y. Lin, *Angew. Chem. Int. Ed.* **2017**, *56*, 13944-13960.

[14] C. Zhu, Q. Shi, S. Feng, D. Du, Y. Lin, *ACS Energy Lett.* **2018**, *3*, 1713-1721.

[15] X. Li, X. Yang, Y. Huang, T. Zhang, B. Liu, *Adv. Mater.* **2019**, *31*, 1902031.

[16] F. Zhang, Y. Zhu, Q. Lin, L. Zhang, X. Zhang, H. Wang, *Energy Environ. Sci.* **2021**, *14*, 2954-3009.

[17] J. Cai, R. Javed, D. Ye, H. Zhao, J. Zhang, *J. Mater. Chem. A* **2020**, *8*, 22467-22487.

[18] T. Ling, T. Zhang, B. Ge, L. Han, L. Zheng, F. Lin, Z. Xu, W.-B. Hu, X.-W. Du, K. Davey, S.-Z. Qiao, *Adv. Mater.* **2019**, *31*, 1807771.

[19] J. Kim, H. Jung, S.-M. Jung, J. Hwang, D. Y. Kim, N. Lee, K.-S. Kim, H. Kwon, Y.-T. Kim, J. W. Han, J. K. Kim, *J. Am. Chem. Soc.* **2021**, *143*, 1399-1408.

[20] H. Jin, X. Liu, S. Chen, A. Vasileff, L. Li, Y. Jiao, L. Song, Y. Zheng, S.-Z. Qiao, *ACS Energy Lett.* **2019**, *4*, 805-810.

[21] K. L. Zhou, Z. Wang, C. B. Han, X. Ke, C. Wang, Y. Jin, Q. Zhang, J. Liu, H. Wang, H. Yan, *Nat. Commun.* **2021**, *12*, 3783.

[22] Z. Liu, L. Zeng, J. Yu, L. Yang, J. Zhang, X. Zhang, F. Han, L. Zhao, X. Li, H. Liu, W. Zhou, *Nano Energy* **2021**, *85*, 105940.

[23] H. Sun, C.-W. Tung, Y. Qiu, W. Zhang, Q. Wang, Z. Li, J. Tang, H.-S. Chen, C. Wang, H. M. Chen, *J. Am. Chem. Soc.* **2022**, *144*, 1174-1186.

[24] Y.-R. Hong, S. Dutta, S. W. Jang, O. F. N. Okello, H. Im, S.-Y. Choi, J. W. Han, I. S. Lee, *J. Am. Chem. Soc.* **2022**, *144*, 9033-9043.

[25] R. Subbaraman, D. Tripkovic, D. Strmcnik, K.-C. Chang, M. Uchimura, A. P. Paulikas, V. Stamenkovic, N. M. Markovic, *Science* **2011**, *334*, 1256-1260.

[26] S.-Y. Bae, J. Mahmood, I.-Y. Jeon, J.-B. Baek, *Nanoscale Horiz.* **2020**, *5*, 43-56.

[27] S. Zhang, J. Li, E. Wang, *ChemElectroChem* **2020**, *7*, 4526-4534.

[28] X. Cao, J. Huo, L. Li, J. Qu, Y. Zhao, W. Chen, C. Liu, H. Liu, G. Wang, *Adv. Energy Mater.* **2022**, *12*, 2202119.

[29] G. Chen, Y. Zhu, H. M. Chen, Z. Hu, S.-F. Hung, N. Ma, J. Dai, H.-J. Lin, C.-T. Chen, W. Zhou, Z. Shao, *Adv. Mater.* **2019**, *31*, 1900883.

[30] Y. Zhu, G. Chen, Y. Zhong, Y. Chen, N. Ma, W. Zhou, Z. Shao, *Nat. Commun.* **2018**, *9*, 2326.

[31] P. Wang, X. Zhang, J. Zhang, S. Wan, S. Guo, G. Lu, J. Yao, X. Huang, *Nat. Commun.* **2017**, *8*, 14580.

[32] Q. Wu, M. Luo, J. Han, W. Peng, Y. Zhao, D. Chen, M. Peng, J. Liu, F. M. F. de Groot, Y. Tan, *ACS Energy Lett.* **2020**, *5*, 192-199.

[33] A. J. Bard, L. R. Faulkner, *Electrochem.* **2001**, *2*, 580-632.

[34] G. Huang, W. Liang, Y. Wu, J. Li, Y. Q. Jin, H. Zeng, H. Zhang, F. Xie, J. Chen, N. Wang, Y. Jin, H. Meng, *J. Catal.* **2020**, *39*, 23-29.

[35] X. Tian, P. Zhao, W. Sheng, *Adv. Mater.* **2019**, *31*, 1808066.

[36] Y. Zhu, G. Chen, X. Xu, G. Yang, M. Liu, Z. Shao, *ACS Catal.* **2017**, *7*, 3540-3547.

[37] Y. Zhu, H.-C. Chen, C.-S. Hsu, T.-S. Lin, C.-J. Chang, S.-C. Chang, L.-D. Tsai, H. M. Chen, *ACS Energy Lett.* **2019**, *4*, 987-994.

[38] Y. Zhu, T.-R. Kuo, Y.-H. Li, M.-Y. Qi, G. Chen, J. Wang, Y.-J. Xu, H. M. Chen, *Energy Environ. Sci.* **2021**, *14*, 1928-1958.

[39] Y. Zhu, G. Chen, Y.-C. Chu, C.-S. Hsu, J. Wang, C.-W. Tung, H. M. Chen, *Angew. Chem. Int. Ed.* **2022**, *134*, e202211142.

[40] Q. He, Y. Zhou, H. Shou, X. Wang, P. Zhang, W. Xu, S. Qiao, C. Wu, H. Liu, D. Liu, S. Chen, R. Long, Z. Qi, X. Wu, L. Song, *Adv. Mater.* **2022**, *34*, 2110604.

[41] A. Suzuki, A. Yamaguchi, T. Chihara, Y. Inada, M. Yuasa, M. Abe, M. Nomura, Y. Iwasawa, *J. Phys. Chem. B* **2004**, *108*, 5609-5616.

[42] K. Mori, R. Osaka, K. Naka, D. Tatsumi, H. Yamashita, *ChemCatChem* **2019**, *11*, 1963-1969.

[43] L, Fu, Y. Li, N, Yao, F. Yang, G. Cheng, W. Luo, *ACS Catal.* **2020**, *10*, 7322-7327.

[44] W. Zhong, B. Xiao, Z. Lin, Z. Wang, L. Huang, S. Shen, Q. Zhang, L. Gu, *Adv. Mater.* **2021**, *33*, 2007894.

[45] Q. He, D. Tian, H. Jiang, D. Cao, S. Wei, D. Liu, P. Song, Y. Lin, L. Song, *Adv. Mater.* **2020**, *32*, 1906972.

[46] Z. Li, W. Niu, Z. Yang, A. Kara, Q. Wang, M. Wang, M. Gu, Z. Feng, Y. Du, Y. Yang, *Energy Environ. Sci.* **2020**, *13*, 3110-3118.

Sodium cobalt oxide substrate provides active sites for dissociation of water, and the generated H intermediates recombine to generate H_2 on the Ru single atoms or clusters. Comparing the two kinds of Ru sites, Ru cluster dominates the alkaline HER activity due to the more fluent migration of H intermediates and its more favorable adsorption-desorption energetics towards H intermediates.

Yanping Zhu, Ke Fan, Chia-Shuo Hsu, Gao Chen, Changsheng Chen, Tiancheng Liu, Zezhou Lin, Sixuan She, Liuqing Li, Hanmo Zhou, Ye Zhu, Hao Ming Chen, Haitao Huang**

Supported Ruthenium Single-Atom and Clustered Catalysts Outperform Benchmark Pt for Alkaline Hydrogen Evolution